Cooling of the wintertime Arctic stratosphere induced by the Western Pacific teleconnection pattern

Kazuaki Nishii (nishii@eps.s.u-tokyo.ac.jp)

Hisashi Nakamura (hisashi@eps.s.u-tokyo.ac.jp)

Graduate School of Science, The University of Tokyo, Tokyo, Japan

7-3-1 Hongo Bunkyo-ku Tokyo, 113-0033, Japan

Yvan J. Orsolini (orsolini@nilu.no)

Norwegian Institute for Air Research, Kjeller, Norway; also at Bjerknes Centre for Climate Research, Norway

NILU, PO Box 100, N-2027 Kjeller, Norway

Abstract

A composite analysis for extreme positive events of the Western Pacific (WP) teleconnection pattern with blocking flow configurations observed over the subpolar Far East shows that such an event in winter can trigger a persistent cold period in the polar stratosphere and, if it occurs in fall or early winter, it augments the possibility of the formation of polar stratospheric clouds. The stratospheric cooling occurs in conjunction with the weakening of upper-tropospheric planetary waves and their upward propagation into the stratosphere soon after the peak time of the WP pattern. Synoptically, this weakening of the upper-tropospheric planetary waves is manifested as westward evolution of a developing blocking high into the climatological-mean pressure trough over the subpolar Far East. This study thus presents a unique case where a blocking high can induce cooling in the polar stratosphere rather than warming.

1. Introduction

The Western Pacific pattern (WPP) is a major teleconnection pattern in the wintertime troposphere and characterized by a meridional dipole of circulation anomalies over the Far East and North Pacific [*Wallace and Gutzler,* 1981]. Remote atmospheric responses to El Niño/Southern Oscillation (ENSO) are known to have a considerable projection onto WPP [*Horel and Wallace,* 1981]. During a month when the

WPP index is positive, blocking highs tend to occur more frequently over the North Pacific than in the climatological situation [*Pavan et al.,* 2000]. Thus WPP exerts a substantial impact on weather and climatic conditions over the Far East and North Pacific, including its influence on storm-track activity [*Nakamura et al.,* 1987; *Lau*, 1988] and cold-air outbreaks [*Takaya and Nakamura* 2005].

The influence of WPP is not limited to the troposphere. *Orsolini et al*. [2009] have revealed that the expansion of an extremely cold domain over the Arctic where Polar Stratospheric Clouds (PSCs) can potentially form tends to follow a tropospheric positive WPP event (WPPE) that occurs about a month earlier. The expansion is in correlation with the reduction of upward injection of planetary-wave (PW) activity into the stratosphere, and it is consistent with the tendency for a blocking high over the western North Pacific (WNP) to lead to the intensification of the stratospheric polar vortex [*Woollings et al.,* 2010]. In fact, in recent composite analyses for events of polar vortex intensification (VI), one may notice a tropospheric anticyclonic anomaly over the subpolar Far East, which is reminiscent of WPP at the mature stage of VI events [*Limpasuvan et al.,* 2005] or a month earlier [*Kolstad and Charlton,* Observed and simulated precursors of stratospheric polar vortex anomalies in the Northern Hemisphere, submitted to *Climate Dynamics*, 2010]. One may also notice that a tropospheric anomaly pattern that possibly includes a signature of blocking and exhibits strong co-variability with the stratospheric polar vortex, revealed through rotated singular value decomposition analysis by *Cheng and Dunkerton* [1995], has a substantial projection onto WPP.

The aim of this study is to present typical daily evolution of the positive WPP and the subsequent cooling in the Arctic stratosphere through composite analysis. We also perform a case study for the 1995/96 winter, when the potential area of PSC formation was particularly large [e.g. *Pawson and Naujokat*, 1999]. In addition, mechanisms for the stratospheric cooling induced by the positive WPP are elucidated from a viewpoint of interference between the climatological-mean PWs and an anomalous Rossby wave packet.

2. Data and analysis method

The Japanese 25-year Reanalysis (JRA-25) [*Onogi et al.*, 2007] from 1979 through 2008 is used. We focus on quasi-stationary anomalies that have been extracted with a digital filter by retaining fluctuations with periods longer than 8 days in the original time series. Daily climatological-mean fields have been constructed for the period 1980-2003 based on 31-day running mean fields. Anomalies are defined locally as departures of the 8-day low-pass-filtered daily fields from the daily climatology for the corresponding calendar days.

To identify typical WPP anomalies, an Empirical Orthogonal Function (EOF) analysis was applied to monthly anomaly fields of 500-hPa geopotential height for the winters (NDJFM) from 1979/80 through 2007/08 over the WNP (20°N-70°N, 120°E-180°). The first EOF, regarded as WPP in this study, accounts for 34% of the total height variance within the domain. The positive phase of WPP is defined as the situation in which the subpolar anomaly is anticyclonic. The daily WPP index has been obtained by projecting the daily low-pass-filtered 500-hPa height anomaly fields onto the WPP anomaly pattern based on the EOF. On the basis of the daily index, the 18 strongest positive WPPEs have been selected for our analysis. At the peak time of each of the events, the index value exceeds three standard deviations. Poleward eddy heat flux at the 100-hPa level averaged poleward of 45°N is used as an indicator of an upward flux of extratropical PW activity from the troposphere. If zonally averaged, the heat flux is equivalent to the vertical component of the conventional Eliassen-Palm flux, and enhancement of the heat flux has been shown to weaken the stratospheric polar vortex [*e.g., Polvani and Waugh*, 2004]. We estimated the heat flux anomaly ($[V^*T^*]_a$) from the low-pass-filtered fields of meridional wind velocity (V) and temperature (T) with a subscript a for anomaly. Asterisks signify the eddy components as deviations from their zonal means and square brackets the zonal averaging.

3. A case study

As a typical example, a prominent positive WPPE observed in the 1995/96 winter is discussed in this section. It was the third strongest event within the entire analysis period, and at its peak time the WPP index reached as much as four standard deviations (black line in Figure 1c). Figure 1a shows the time-height evolution of temperature anomalies averaged over the Arctic (poleward of 70°N), and the evolution of lower-stratospheric (50-hPa) temperature anomaly is highlighted in Figure 1c with a red line. In the upper and middle stratosphere (above the 30-hPa level), the temperature dropped rapidly at the beginning of December. The cool anomaly then spread downward to reach the bottom of the stratosphere (around the 300-hPa level) by the end of the month. In the middle and lower stratosphere, the cool anomaly persisted until the end of March, whereas in the upper stratosphere (above the 10-hPa level), a warm anomaly developed in mid-January and then spread gradually downward (not shown). The downward evolution of stratospheric temperature anomalies is known to appear in association with the Northern Annular Mode [*Baldwin and Dunkerton*, 1999]. The 50-hPa cooling occurred in conjunction with the weakening of zonal wavenumber one (k=1) component of stratospheric PWs (blue line). *Pawson and Naujokat* [1999] showed that the potential PSC formation area, where the 50-hPa temperature is below 195 K, started to expand anomalously in mid-December.

As pointed out by *Takaya and Nakamura* [2005], the daily evolution of a positive WPPE is similar to that of a blocking high over the subpolar WNP. In fact, Figure 2i shows that 250-hPa Ertel's potential vorticity (PV) field observed on November 25, five days prior to the peak time of the event, was characterized by a prominent blocking ridge with low PV around the date line. For the following five days, the upper-tropospheric pressure ridge developed westward into the high-PV area of the climatological pressure trough over the Far East yielding a cyclonic breaking locally (Figure 2j). As shown by a green line in Figure 1c, marked weakening was observed in the k=1 component, which is dominant climatologically in the upper-tropospheric PW field. Upward PW propagation was thus suppressed in late November, as indicated by negative $[V^*T^*]_a$ (black line in Figure 1e) just before the beginning of the stratospheric cooling. Our finding is consistent with *Orsolini et al*. [2009], who showed that the positive WPP weakens upward propagation of PWs by reducing their amplitude by the superposition of an anticyclonic anomaly on the climatological-mean trough over the Far East.

4. Composite analysis

To generalize the results obtained through the case study for the 1995/96 winter, we have constructed composite maps for the 18 prominent positive WPPEs relative to their peak times. Figure 1b shows a height-time section of the composited evolution of polar temperature anomalies, which looks quite similar to the corresponding evolution in the 1995/96 winter (Figure 1a). Soon after the peak time of a WPPE, the upper- and mid-stratospheric temperature anomaly turns negative, and this cooling signal rapidly spreads downward into the lower stratosphere within five days. This cold anomaly persists for about a month, while a warm anomaly appears in the upper stratosphere ~20 days after the peak time. The polar cooling accompanies the intensification of the westerly polar-night jet (not shown). In the composite evolution, the rapid stratospheric cooling occurs concurrently with a significant reduction in the 100-hPa upward flux of PW activity (black line in Fig. 1f). The reduction, as represented by negative $[V^*T^*]_a$, becomes strongest 1 day after the peak time.

In the troposphere (Figures 2e-f), the positive WPP accompanies a dipolar height anomaly pattern (black contours and shading) with an anticyclonic blocking ridge (purple contour) that evolves westward. This evolution corresponds to cyclonic breaking of the PW trough over the WNP. This breaking signature is more striking in the PV map composited for the peak time (Figure 2k), which is remarkably similar to the corresponding one in the 1995 event (Figure 2j). As shown by a green line in Figure 1d, the breaking weakens the k=1 component of the upper-tropospheric PWs.

As evident in a zonal-height section of height anomalies at 60°N (Figure 2l), both the tropospheric blocking anomaly and the associated cyclonic anomaly downstream over North America are deep, extending into the stratosphere. At the peak time, the respective anomalies in the stratosphere are located to the west and east of the climatological Aleutian high (Figure 2b). The high (or pressure ridge in the total PW field) is initially recognized as a poleward meander of geopotential height contours (purple lines in Figure 2a). For the next five days (Figure 2c), the ridge breaks down through its destructive interference with the westward-developing cyclonic *anomaly*. Although the stratospheric anomaly field is dominated by the k=1 component, its zonal phase is such that it weakens the total PW field. The polar vortex thus becomes remarkably annular (Figure 2c) under the diminished PW signature (black line in Figure 1f), and correspondingly a cool anomaly develops rapidly in the Arctic stratosphere (red line in Figure 1d). The signal of the tropospheric WPP almost diminishes 20 days after its peak time, but the cool, cyclonic anomaly in the stratosphere associated with the intensified polar vortex still retains its intensity even 20 days after the peak time (Figures 2d and 2h).

5. Mechanisms for the weakening of stratospheric PWs

In this section, we examine in detail how the destructive interference occurs between the climatological-mean PWs and the stratospheric anomalies induced by the tropospheric WPP. *Nishii et al.* [2009] showed that anomalous waves are often observed in the form of a zonally-confined Rossby wave packet propagating three-dimensionally. In fact, a wave-activity flux diagnosis [*Takaya and Nakamura*, 2001] applied to the composited 100-hPa anomaly fields reveals that the tropospheric anticyclonic anomaly releases Rossby wave activity upward into the stratosphere (green contours in Figures 2a-c). The upward-propagating wave-packet structure can be recognized in the zonal-height section (Figure 2l) as westward-tilting phase lines of the height anomalies. We have decomposed 100-hPa $[V^*T^*]_a$ into individual contributions from $[V_a^*T_c^*]$, $[V_c^*T_a^*]$ and $[V_a^*T_a^*]_a$ (green, blue and red lines, respectively, in Figures 1e-f). Here, the subscript *c* is for climatology. The terms $[V_a^*T_c^*]$ and $[V_c^*T_a^*]$ represent contributions from the interference between the climatological-mean PWs and anomalous waves, whereas $[V_a^*T_a^*]_a$ represents an anomalous instantaneous contribution from upward-propagating wave packets. Section 2 of *Nishii et al.* [2009] should be referred to for more details.

Both in the 1995 event (Figure 1e) and in the composite (Figure 1f), the weakening of

$[V^*T^*]_a$ is mainly due to $[V_a^*T_c^*]$ and $[V_c^*T_a^*]$. The weakening of $[V^*T^*]_a$ in late November 1995 was contributed to also by weakned wave-packet propagation ($[V_a^*T_a^*]_a$) (Figure 1e). Consistently with the upward propagation of anomalous waves, the wave-packet term $[V_a^*T_a^*]_a$ in the composite is positive, but not significant (Figure 1f). Thus it cannot offset the effect of destructive interference between the climatological PW trough and the anticyclonic anomaly associated with the positive WPP, as indicated by negative of $[V_a^*T_c^*]$ and $[V_c^*T_a^*]$.

To gain a deeper insight into the reduced upward PW propagation, we plot the distribution of 100-hPa V^* and T^*. Figure 3a shows the climatological situation where positive V_c^* (southerlies) overlaps warm T_c^* over the WNP as a manifestation of the upward propagation of the climatological-mean PWs. In the composited maps for the peak time of the positive WPPEs (Figure 3b), poleward V^* accompanying warm T^* over the Far East contributes positively to $[V^*T^*]_a$, which is, however, counteracted by a negative contribution from equatorward V^* with warm T^* over Alaska and the Bering Sea, in addition to poleward V^* with cool T^* over Greenland. This negative contribution is attributable to the interference between the climatological-mean PWs and anomalies associated with the WPP, to which $[V^*_a T^*_c]$ contributes dominantly (Figure 1f). In fact, Figure 3c indicates that anomalous meridional wind is strongly equatorward ($V_a^* <0$)

over the Alaska-Bering sector, where it is climatologically warm (T_c* >0). Due to their destructive interference with the anomalous waves, the PWs in the subpolar region becomes less baroclinic with their phase lines becoming nearly vertical and virtually no longitudinal correlation between V* and T* (not shown). The upward PW propagation is thus diminished around the peak time of a WPPE. For the next few days, the V*-T* correlation gradually recovers but their amplitudes are reduced substantially (Figures 2c and 2g).

6. Summary and discussion

In this study, we have shown that a positive WPPE in winter can be a precursor for one-month lasting polar stratospheric cooling up to 6 K, revealing their dynamical linkage. The positive WPP weakens upward PW propagation into the stratosphere through the destructive interference between the climatological PWs and wavy anomalies associated with WPP. In *Orsolini et al.* [2009], monthly events of extreme PSC volume tend to be observed in the following months of the positive WPP. Most of the positive WPPEs in the October-January period used for our compositing were followed by the largest PSC area events at the 50-hPa level, but none of those events in February or March were. In fact, the 50-hPa field composited for 20 days after the peak time of those 9 events that were observed in fall or early winter (October-January) shows a domain of temperature below 195K (blue contour in Figure 2d). This seasonality is understandable, since the PSC formation depends more directly on temperature itself than on its anomaly and the PSC area thus tends to maximize in midwinter (i.e., January or February). The present study has shown that extreme midwinter coolness in the Arctic stratosphere can be triggered by an extreme positive WPPE in fall or early winter (October-January).

The daily evolution of the positive WPP is quite similar to the development of a blocking high over the WNP [e.g., *Takaya and Nakamura*, 2005]. Thus, this study presents a unique case where a blocking high can induce cooling in the polar stratosphere rather than warming. In fact, the positive contribution $[V^*_a T^*_a]_a$, which is consistent with a general tendency for blocking highs to act as precursors of stratospheric sudden warming events (*e.g.*, *Martius et al.* [2009]), is modest even for strong blocking events associated with the WPP. As their unique dynamical characteristic, the contribution is overwhelmed by the destructive interference between the blocking anomaly and climatological-mean PWs.

Climatologically, upward PW propagation into the stratosphere is strongest over the WNP [*Plumb*, 1985], where circulation anomalies can therefore potentially modify the upward PW propagation efficiently. Nevertheless, correlation between the WPP index and 50-hPa polar temperature anomaly for winter (NDJFM) is not particularly strong (at most -0.17 with the lag of 9 days). The weak correlation reflects the fact the stratospheric variability is not determined solely by WPPEs, but it may also reflect the tendency for negative WPPEs to accompany insignificant stratospheric warming (not shown).

Acknowledgments

Comments by Dr. T. J. Dunkerton and an anonymous referee are invaluable. KN and HN have been supported by the Japanese Ministry of Education, Culture, Sports, Science and Technology under the Grant-in-Aids for Scientific Research (A) #18204044 and (B) #22340135 and by the Ministry of Environment under the Global Environment Research Fund (S-5). YO has been supported by the Norwegian Research Council. The JRA-25 dataset is provided by the Japan Meteorological Agency and the Central Research Institute of Electric Power Industry.

References

Baldwin, M. P., and T. J. Dunkerton (1999), Propagation of the Arctic Oscillation from the stratosphere to the troposphere, *J. Geophys. Res.*, *104*, 30937-30946.

Cheng, X., and T. J. Dunkerton (1995), Orthogonal rotation of spatial patterns derived from singular value decomposition analysis, *J. Clim.*, *8*, 2631-2643.

Horel, J. D., and J. M. Wallace (1981), Planetary-scale atmospheric phenomena associated with the Southern Oscillation, *Mon. Weather Rev.*, *109*, 813-829.

Lau, N. C. (1988), Variability of the observed midlatitude storm tracks in relation to low-frequency changes in the circulation pattern, *J. Atmos. Sci.*, *45*, 2718-2743.

Limpasuvan, V., D. L. Hartmann, D. W. J. Thompson, K. Jeev, and Y. L. Yung (2005), Stratosphere-troposphere evolution during polar vortex intensification, *J. Geophys. Res.*, *110*, D24101, doi:10.1029/2005JD006302.

Martius, O., L. M. Polvani, and H. C. Davies (2009), Blocking precursors to stratospheric sudden warming events, *Geophys. Res. Lett.*, *36*, L14806, doi:10.1029/2009GL038776.

Nakamura, H., M. Tanaka, and J. M. Wallace (1987), Horizontal structure and energetics of Northern Hemisphere wintertime teleconnection patterns, *J. Atmos. Sci.*, *44*, 3377-3391.

Nishii, K., H. Nakamura, and T. Miyasaka (2009), Modulations in the planetary wave field induced by upward-propagating Rossby wave packets prior to stratospheric sudden warming events: A case study, *Q. J. R. Meteorol. Soc.*, *135*, 39-52.

Onogi, K., et al. (2007), The JRA-25 reanalysis, *J. Meteorol. Soc. Jpn.*, *85*, 369-432.

Orsolini, Y. J., A. Y. Karpechko, and G. Nikulin (2009), Variability of the Northern Hemisphere polar stratospheric cloud potential: The role of North Pacific disturbances, *Q. J. R. Meteorol. Soc.*, *135*, 1020-1029.

Pavan, V., S. Tibaldi, and C. Brankovic (2000), Seasonal prediction of blocking frequency: Results from winter ensemble experiments, *Q. J. R. Meteorol. Soc.*, *126*, 2125-2142.

Pawson, S., and B. Naujokat (1999), The cold winters of the middle 1990s in the northern lower stratosphere, *J. Geophys. Res.*, *104*, 14209-14222.

Plumb, R. A. (1985), On the three-dimensional propagation of stationary waves, *J. Atmos. Sci.*, *42*, 217-229.

Polvani, L. M., and D. W. Waugh (2004), Upward wave activity flux as a precursor to extreme stratospheric events and subsequent anomalous surface weather regimes, *J. Clim.*, *17*, 3548–3554.

Takaya, K., and H. Nakamura (2001), A formulation of a phase-independent wave-activity flux of stationary and migratory quasi-geostrophic eddies on a zonally varying basic flow, *J. Atmos. Sci.*, *58*, 608-627.

Takaya, K., and H. Nakamura (2005), Geographical dependence of upper-level blocking formation associated with intraseasonal amplification of the Siberian high, *J. Atmos.*

Sci., *62*, 4441-4449.

Wallace, J. M., and D. S. Gutzler (1981), Teleconnections in the geopotential height field during the Northern Hemisphere winter, *Mon. Weather Rev.*, *109*, 784-812.

Woollings, T., A. J. Charlton-Perez, S. Ineson, A. G. Marshall, and G. Masato (2010), Associations between stratospheric variability and tropospheric blocking, *J. Geophys. Res.*, *115*, D06108, doi:10.1029/2009JD012742.

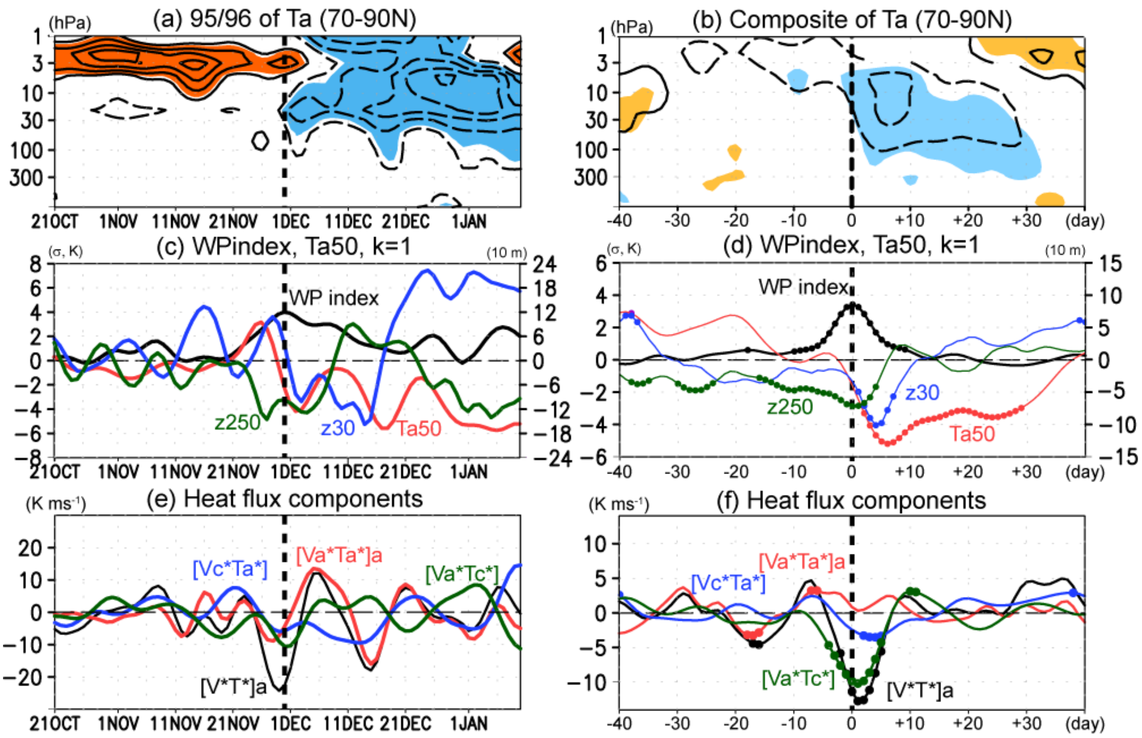

Figure 1. (a) Height-time section of temperature anomaly averaged over the Arctic (poleward of 70°N) from October 20, 1995 through January 10, 1996. Orange and blue shading denotes the absolute values of the anomaly that exceed 4 K positively and

negatively, respectively. Contour interval is 3 K. (b) As in (a), but for the composite for the 18 positive WPPEs. Yellow and blue shading denotes the composited anomalies significantly positive and negative, respectively, at the 95% confidence level with the t-statistic. (c) Daily time series (1995/96 winter) of the WPP index (black; left axis), 50-hPa temperature anomaly averaged over the Arctic (red; left axis), anomalous amplitude of the k=1 component of PW in 250-hPa height (green; right axis) and 30-hPa height (blue; right axis) at 50°N. (d) As in (c), but for the corresponding time series based on the composite for the positive WPPEs. Dots denote the anomalies significant at the 95% confidence level. (e) Daily time series (1995/96 winter) of contributions to 100-hPa eddy heat flux (K m s^{-1}) from $[V^*T^*]_a$ (black), $[V_a^*T_c^*]$ (green), $[V_c^*T_a^*]$ (blue) and $[V_a^*T_a^*]_a$ (red), averaged poleward of 45°N. (f) As in (e), but for the corresponding time series based on the composite for the positive WPPEs.

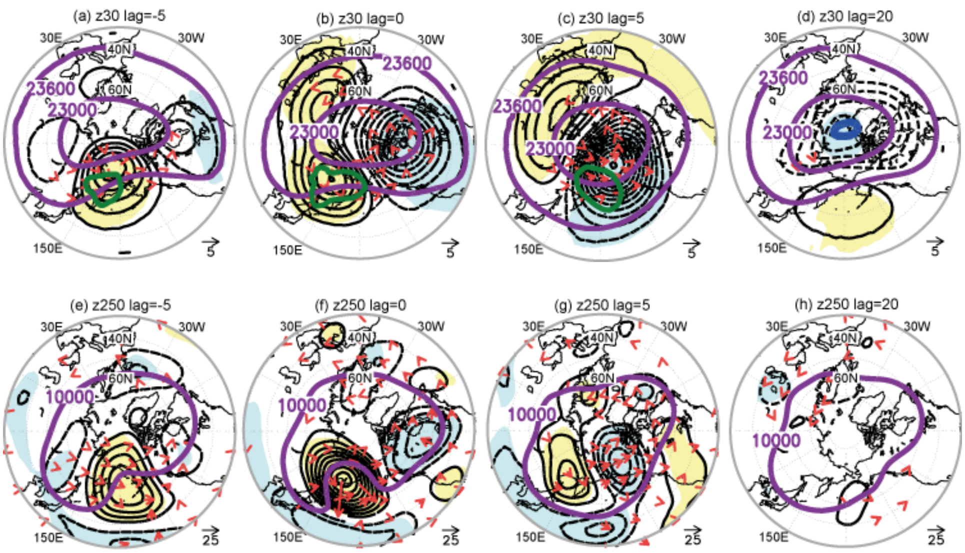

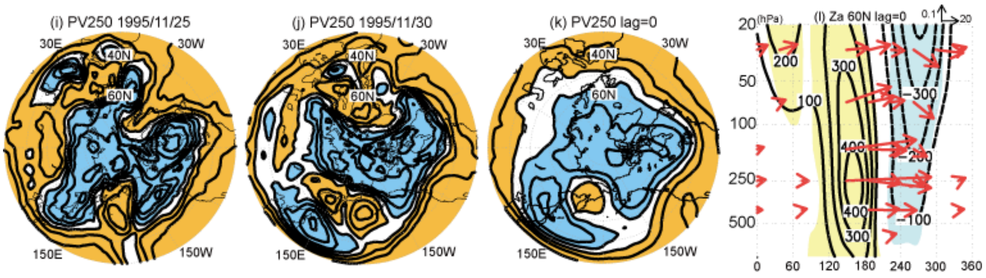

Figure 2. (a-d) Polar stereographic maps (poleward of 30°N) of 30-hPa height anomalies composited for the 18 positive WPPEs (black lines) with lags of (a) -5, (b) 0, (c) +5 and (d) +20 days relative to their peak time. Contour interval is 50 m (dashed for negative; zero lines omitted). Yellow and blue shading denotes positive and negative anomalies, respectively, significant at the 95% confidence level. Purple lines indicate composited 30-hPa height of 23000 and 23600m, arrows the 30-hPa horizontal component of Rossby wave-activity flux (unit; m^2s^{-2}), and green lines 100-hPa upward component of the flux of 0.005 m^2s^{-2}. In the area encircled by the blue contour in (d), 50-hPa temperature composited for the 9 positive WPPEs in the October-January period is below 195 K. (e-h) As in (a-d), but for 250-hPa height anomalies. Purple contours represent composited 250-hPa height of 10000m. (i, j) 250-hPa Ertel's PV on November (i) 25 and (j) 30, 1995 (black; contour interval is 1 PVU) with blue shading for 4 PVU or higher and yellow shading for 3 PVU or lower. (k) As in (i), but for PV composited for the peak times of the 18 positive WPPEs. (l) Zonal height section for 60°N of height

anomalies composited for the peak times of the 18 positive WPPEs. Yellow and blue shading denotes positive and negative anomalies, respectively, significant at the 95% confidence level. Arrows represent the zonal and vertical components of the Rossby wave-activity flux (m^2s^{-2}).

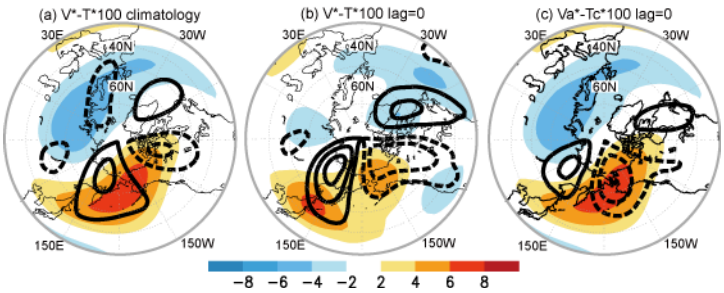

Figure 3. (a) Winter (NDJFM) climatology of eddy components of 100-hPa meridional wind velocity (V_c*; contoured for every 5 m s^{-1}; dashed for the northerlies) and temperature (T_c*; shaded as indicated below if warmer and cooler, respectively, than the longitudinal average; interval: 2 K). (b) As in (a), but for V* and T* composited for the peak times of the 18 positive WPPEs. (c) As in (b), but for anomalous meridional wind (V_a*) and climatological-mean temperature (T_c*) that contribute to [V_a*T_c*].